energies

MDPI

Article

Experimental Optimization of Passive Cooling of a Heat Source Array Flush-Mounted on a Vertical Plate

Antoine Baudoin [1,*], Didier Saury [2], Bo Zhu [2] and Cecilia Boström [1]

[1] Division for Electricity, Uppsala University, Box 534, 751 21 Uppsala, Sweden; Cecilia.Bostrom@angstrom.uu.se

[2] Institut PPRIME, CNRS, ENSMA, Université de Poitiers, BP 40109, F-86961 Futuroscope Chasseneuil CEDEX, France; didier.saury@ensma.fr (D.S.); bo.zhu@etu.isae-ensma.fr (B.Z.)

* Correspondence: antoine.baudoin@angstrom.uu.se; Tel.: +46-18-471-5870

Academic Editor: Maurizio Sasso

Received: 12 July 2016; Accepted: 1 November 2016; Published: 4 November 2016

Abstract: Heat sources, such as power electronics for offshore power, could be cooled passively—mainly by conduction and natural convection. The obvious advantage of this strategy is its high reliability. However, it must be implemented in an efficient manner (i.e., the area needs to be kept low to limit the construction costs). In this study, the placement of multiple heat sources mounted on a vertical plate was studied experimentally for optimization purposes. We chose a regular distribution, as this is likely to be the preferred choice in the construction process. We found that optimal spacing can be determined for a targeted source density by tuning the vertical and horizontal spacing between the heat sources. The optimal aspect ratio was estimated to be around two.

Keywords: discrete heat sources; source array; natural convection; optimization

1. Introduction

The energy from the oceans can be extracted by offshore wind power, wave power, tidal power, tidal marine currents, temperature gradients, and salinity gradients. For wave power, the potential is estimated to be 8000 TWh/year–80,000 TWh/year [1]. There exist a significant number of different wave energy conversion technologies [2]. Offshore technologies require a power conversion system before transmission to shore, in order to ensure a high power quality to the grid [3]. The conversion system usually consists of passive and active converters in different power electronics topologies; see, for example [4,5]. Offshore operation puts high demands on the reliability and lifetime of the power components, and the maintenance work is expensive compared to onshore installations. A key issue in ensuring a long lifetime of the power components is a strategy for proper cooling of the components [6–8].

Mechanical cooling systems—such as fans or pumps—have a limited lifetime. Hence, for an offshore system, a passive cooling strategy is preferable. Such a strategy is indeed silent, reliable, and cheap. For instance, the optimal spacing between insulated-gate bipolar transistors (IGBTs) installed in a submerged substation for wave power was studied in [9], and showed a necessary trade-off between construction costs and effective cooling. Passive cooling can make use of conventional fins, but also heat pipes [10] or nanomaterials [11] to enhance the cooling capacity. It is used, amongst others, for electronics [12], photovoltaics [13], telecommunications [14], and LED modules [15].

To investigate the feasibility of passive cooling for marine energy systems, an array of heat sources is considered in a simple configuration, where conjugated conduction and natural convection are the dominant heat transfer modes. Natural convection—being a key phenomenon in passive cooling—has received increasing attention for engineering applications in the last decades [16]. Interest

for conjugated natural convection grew with the development of electronics. Miniaturization in microelectronics and the consequent increase in heat flux density made it necessary to optimize cooling. In 1995, an array of identical discrete heat sources was studied numerically and experimentally with conjugated conduction and natural convection [17]. Two-dimensional heat source arrays have been studied numerically in [18] and experimentally in [19,20] in order to maximize the cooling of different heat sources, often by investigating the influence of the placement of the heat sources. Another approach is to optimize the heat distribution at sources with fixed locations [21]. Habib, Sultan, and Rajkumar [22–24] presented an experimental study of heated bands and the one-dimensional optimization of the spacing. In fact, the majority of the literature on heating by discrete sources is restricted to the one-dimensional approach. When dealing with natural convection, one must be aware of the importance of radiative effects [25]. Most of the works described in the following have been declined for mixed or forced convection, as for instance in [26]. A rich body of literature is available when widening the problem to mixed and forced convection, as well as to different geometries, such as enclosures, open cavities, channels, fins, or horizontal configurations. Problems with discrete heating and natural convection have been the subject of several reviews [27,28].

As suggested in [29], a regular distribution is not optimal, but it can still be preferred in an industrial context, in order to simplify the production process. The present study tries to answer the optimization problem of placing identical heat sources on a vertical plate with a high density, whilst keeping the passive cooling as efficient as possible. The optimization strategy has been fully experimental, rather than indirect through validation of a model. This was achieved by designing a setup which allowed for the testing of a large number of distributions. We looked for the vertical and horizontal spacing of a regular grid. This study addresses a need in wave power, and the setup matches the typical conditions encountered by offshore power devices (no/low radiative effects, dimensions, simplicity of the design, type of heaters, open/distant boundaries). However, the results have a general validity, and could be valuable in other applications.

2. Materials and Methods

2.1. Experimental Setup

Figure 1 represents a cut plane of the experimental setup. Nine rectangular heat sources were flush-mounted on one side of a 2 mm-thick vertical metallic plate, whose dimensions are 200 cm in height and 150 cm in width (see also Figure 2 and Table 1). The other side of the plate is free, and cooled by natural convection. The horizontal and vertical spacing between the heat sources—ΔX and ΔY, respectively—can be varied easily. Only regular distributions were considered, with three rows and three columns of heat sources. The metallic plate was made of type 304 stainless steel with a low emissivity of around 0.1.

Table 1. Dimensions of the experimental setup.

Parameter	Value
Metal plate	200 × 150 cm
PCB heating plates (thickness)	5 × 10 cm (1.6 mm)
Thermal sheet thickness	0.2 mm
Polyurethane foam (thickness)	6 × 11 cm (40 mm)
PVC plate (thickness)	6 × 11 cm (5 mm)
Extruded polystyrene thickness	30–40 mm

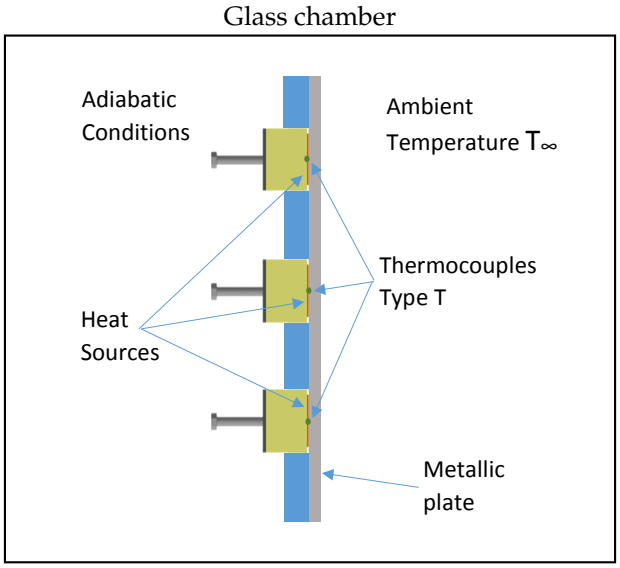

Figure 1. Schematic view of the experimental setup.

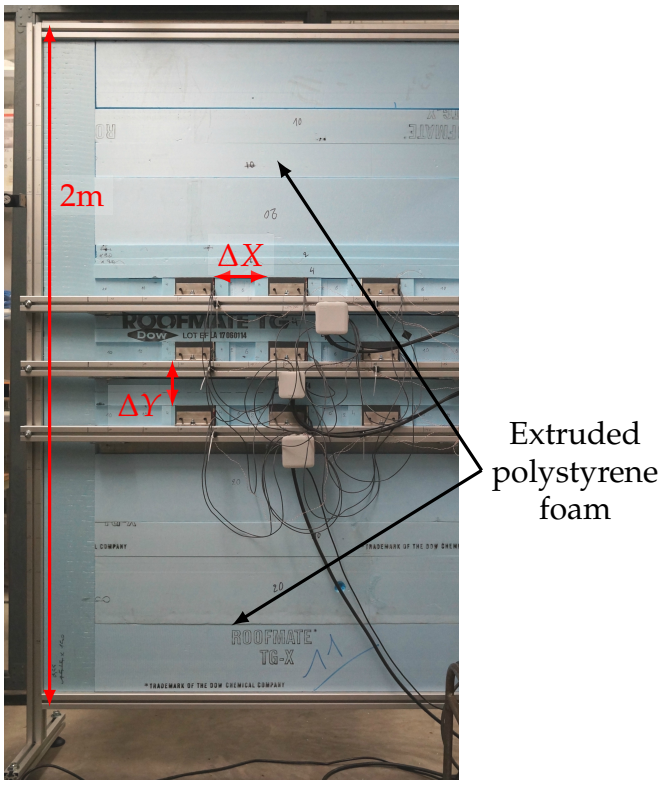

Figure 2. Experimental setup with isolating pieces and structure to change the spacing on the backside of the vertical plate.

The nine heat sources consisted of a 1.6 mm-thick printed copper board (PCB) of 5 cm by 10 cm (typical dimensions for power electronics modules used in marine energy (see, for example 2MBI200U4H-120 IGBT module) with an electrical resistance of around 0.5 Ω. The power at each heat source was initially balanced, and was controlled later by one unique DC-supply unit. The back side of the plate on which the heat sources were mounted was covered by a modular set of pieces of thermal insulating materials, in order to be able to consider this side as adiabatic. This insulating material,

which was in direct contact with the heat sources, was a piece of 40 mm thick polyurethane foam, 6 cm by 11 cm, with a thermal conductivity of 0.028 W/mK, as shown in Figures 1–3. This material was chosen to withstand the high temperature at the heat source. The rest of the insulating parts were made of extruded polystyrene foam with better mechanical properties. This made it easier to manipulate when changing the spacing (thermal conductivity of 0.031 W/mK). A poly(vinyl chloride) (PVC) plate was added on the back of the polyurethane foam in order to apply a uniform mechanical pressure. Pressure was applied with two screws with approximately 0.4 Nm on each.

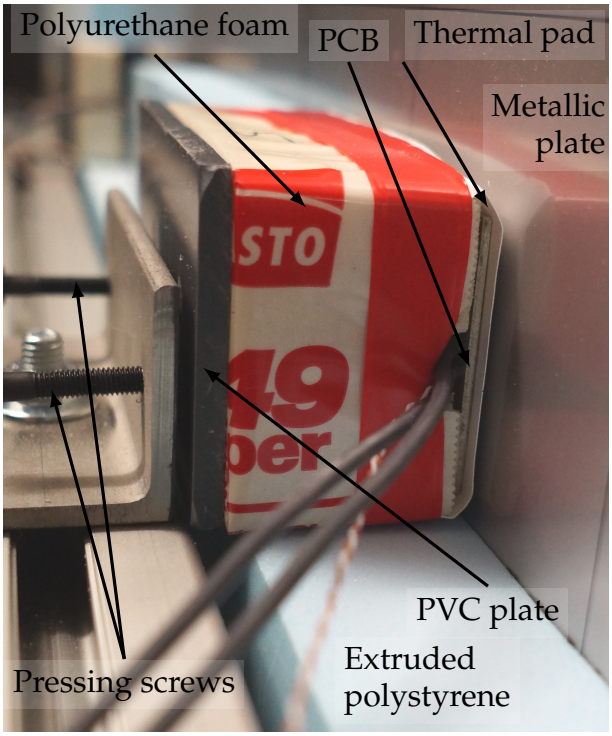

Figure 3. One of the heat sources mounted on the back of the metallic plate.

Between the heat source and the metallic plate, electrically-insulating 0.2 mm-thick thermal pads were used, to avoid electrical short circuits and to enhance the thermal contact. The thermal conductivity of the interface was 7 W/mK.

2.2. Measurements and Procedure

At the centre of each heat source, one thermocouple of type T was installed to measure the temperature. All of the thermocouples were connected to an Agilent 34970 data acquisition unit with two 34901A cards, giving an uncertainty of ± 1 K with an internal compensation using a PT100 sensor. The dissipated power is controlled by the current and the voltage, which were both measured (uncertainty of $\pm 0.02\%$ and $\pm 0.006\%$, respectively). The total dissipated power over the nine heat sources was around 75 W (i.e., averaged heat flux of 1.7 kW/m^2).

The radiative heat flux can therefore be estimated roughly with $\epsilon\sigma(\Delta T^4) < 37$ W/m^2, which is much lower than the total heat flux (see below). Heat losses through the isolated surface of the plate were estimated by measuring the temperature drop over the polyurethane foam, which remained below 4 K, giving a losses flux of $4\lambda/e < 2.7$ W/m^2.

All the tests were performed in a large isolated cell which was inside an air-conditioned room with a constant temperature. The cell was large enough to consider the boundary conditions of the convective phenomenon to be open.

First, the heating system was pressed against the metallic heat sink with a nano-screwdriver to ensure a uniform thermal contact for all the heat sources. The dissipated power was controlled with the DC–power supply unit. The plate was heated until it reached a constant temperature (<1 K/30 min). Due to the thermal expansion, the screws were retightened when the temperature was in a permanent regime. Only steady state was considered in the present study. This procedure was repeated more than 60 times in order to study the influence of vertical and horizontal spacing between the heat sources (see Table 2). The uncertainty on the position was ±1 mm.

Table 2. List of distributions tested.

ΔX	3, 5, 7, 9, 13, 17, 21, 31
ΔY	8, 10, 12, 16, 20, 28, 38, 48

As is common for the characterization of natural convection problems, a Rayleigh number is defined in Equation (1) for the studied configuration. The characteristic length corresponds to the distance between the lower and the upper heat sources. During the tests, Ra ranged from 1×10^8 to 5×10^9.

$$R_a = \frac{g \cdot \beta \cdot \Delta T \cdot (2\Delta Y + 3H)^3}{\nu \cdot \alpha} \tag{1}$$

2.3. Optimal Distributions

The heat transfer modes in the studied problem were dominated by the conduction in the metal plate and the natural convection at the metal–air interface. When sufficiently close to one another, the heat sources heat each other up, and are therefore thermally coupled. The conduction is isotropic (i.e., identical in the horizontal and vertical directions), but the aspect ratio of the heat sources enhances the horizontal thermal coupling. As it is driven by buoyant forces, the convection is anisotropic. Hence, the convective coupling is much stronger in the vertical direction. It is therefore expected that a larger vertical spacing is necessary to obtain an efficient cooling. This study attempts to quantify that effect.

With the measured temperature and the electrical current and voltage, a thermal resistance was defined as shown in Equation (2). Thermal resistance is the quantity of interest in this study, since it indicates the ability of the system to evacuate the dissipated heat. The uncertainty was estimated as shown in Equation (3).

$$R_{th} = \frac{\Delta T}{U \cdot I} \tag{2}$$

$$\frac{\Delta R_{th}}{R_{th}} = \sqrt{\left(\frac{\partial R_{th}}{\partial \Delta T}\frac{1}{R_{th}}\right)^2 + \left(\frac{\partial R_{th}}{\partial UI}\frac{\Delta UI}{R_{th}}\right)^2} = 1.6\% \text{ to } 2.5\% \tag{3}$$

The heat source density is defined in Equation (4). This quantity must be maximized to limit the costs of construction. A density of 1 corresponds to a uniformly-heated plate. When the density tends towards zero, it corresponds to the case of isolated heat sources. The uncertainty was estimated as shown in Equation (5).

$$N = \frac{L \cdot H}{(\Delta X + L) \cdot (\Delta Y + H)} \tag{4}$$

$$\frac{\Delta N}{N} = \sqrt{\left(\frac{\partial N}{\partial \Delta X}\frac{0.001}{N}\right)^2 + \left(\frac{\partial N}{\partial \Delta Y}\frac{0.001}{N}\right)^2} = 0.3\% \text{ to } 1.1\% \tag{5}$$

For efficient cooling, the thermal resistances should be kept as low as possible. In order to optimize the distribution, the heat source density, N, was maximized, and the thermal resistance, R_{th}, was minimized. There are two possible ways to define these optima, $\widetilde{\Delta X}^*$ and $\widetilde{\Delta Y}^*$; see Equation (6) (Method 1) and Equation (7) (Method 2).

$$R_{th}\left(\widetilde{\Delta X}^*_N, \widetilde{\Delta Y}^*_N\right) = min|_{N=constant}\left[R_{th}\left(\Delta X^*, \Delta Y^*\right)\right] \tag{6}$$

$$N\left(\widetilde{\Delta X}^*_{R_{th}}, \widetilde{\Delta Y}^*_{R_{th}}\right) = max|_{R_{th}=constant}\left[N\left(\Delta X^*, \Delta Y^*\right)\right] \tag{7}$$

The results for the central heat source are the most generalizable, and were therefore chosen. This heat source was surrounded by neighbours in all directions in a distribution of nine heat sources. The thermal resistance for this heat source is therefore the best representative of what can be expected for an even larger number of heat sources.

In Method 1, the points on the isolines were obtained by linear interpolation between the two closest measuring points. The isolines for the thermal resistance were fitted numerically according to Equation (8). As such, the parameter c represents the vertical spacing for one single column of heat sources, given a specified thermal resistance. In the same way, b represents the horizontal spacing for a single row of heat sources.

$$(\Delta Y^* + 1) = a \cdot ((\Delta X^* + 1) - b)^{-1} + c \tag{8}$$

Finally, the square root of the derivatives of the density on each isoline was easily found, and gave the optimal positions, presented in Equation (9). Method 2 is similar along an isoline for the density.

$$\widetilde{\Delta X}^* = \sqrt{\frac{a \cdot b}{c}} + d - 1\,;\ \widetilde{\Delta Y}^* = \sqrt{\frac{a \cdot c}{b}} + c - 1 \tag{9}$$

3. Results

3.1. Measurements

The temperature was measured at the centre of each heat source (see Figure 4). Obviously, the temperature increased when the spacing was reduced. For wide spacing, the temperature tended to stabilize. The two higher rows were warmer due to the direction of convective flow, which is oriented upward.

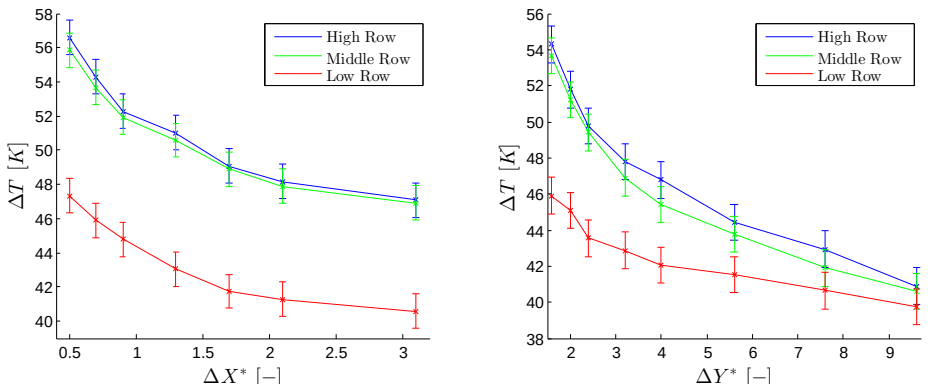

Figure 4. Example of the measured excess temperature averaged on each row of heat sources (**a**) as a function of the horizontal spacing for a fixed vertical one; and (**b**) as a function of the vertical spacing for a fixed horizontal one.

The measurements were used to calculate the thermal resistance, which is presented in Figure 5. The thermal resistance logically increased with the heat source density. For a density above 25%, the thermal resistance doubled. There is no point in continuing the study over this value, as it is unlikely that such a configuration would be chosen in a real case. The rest of the study was therefore restricted to intermediate densities. In this region, the thermal resistance was shown to be proportional to the square root of the heat source density. The linear regression parameters indicated a thermal resistance of approximately 4.7 K/W for an isolated heat source (i.e., zero density, or infinite spacing).

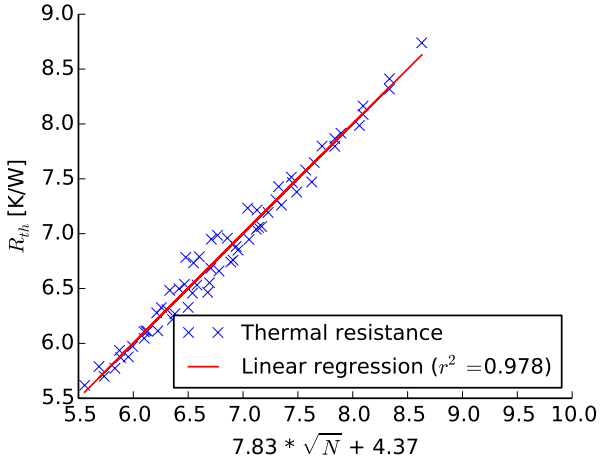

Figure 5. Parity graph for the thermal resistance of the central heat source as a function of the heat source density.

With over 60 distributions tested, the thermal resistance was mapped as a function of the horizontal and vertical spacing (see Figure 6). This Figure shows a comparison between the heat source density (representing the cost) and the thermal resistance for the central heat source.

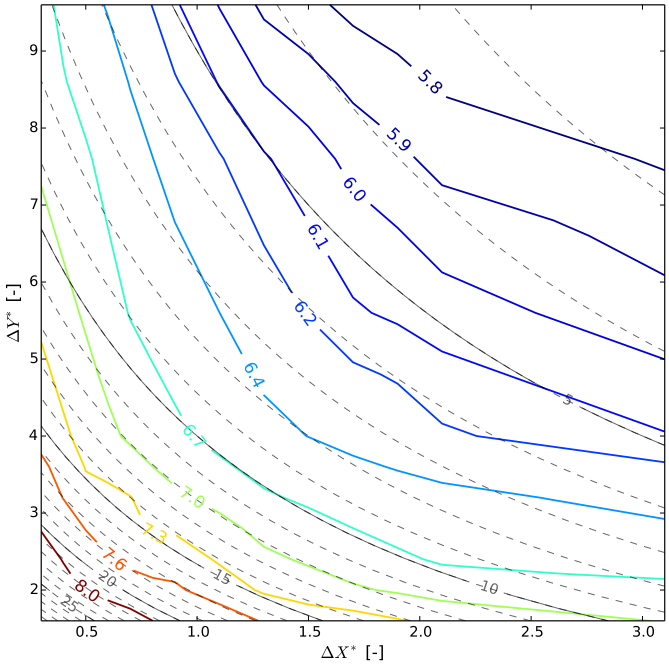

Figure 6. Isolines for the thermal resistance for the central heat source (colored lines) compared to the heat source density (grey lines) as functions of horizontal and vertical spacings.

3.2. Optima

As explained earlier, the optimal positions were calculated based on the measurements for the thermal resistance. Figure 7 shows an example of how the isolines were fitted to give this optimal spacing. The two methods mentioned in the previous section are presented.

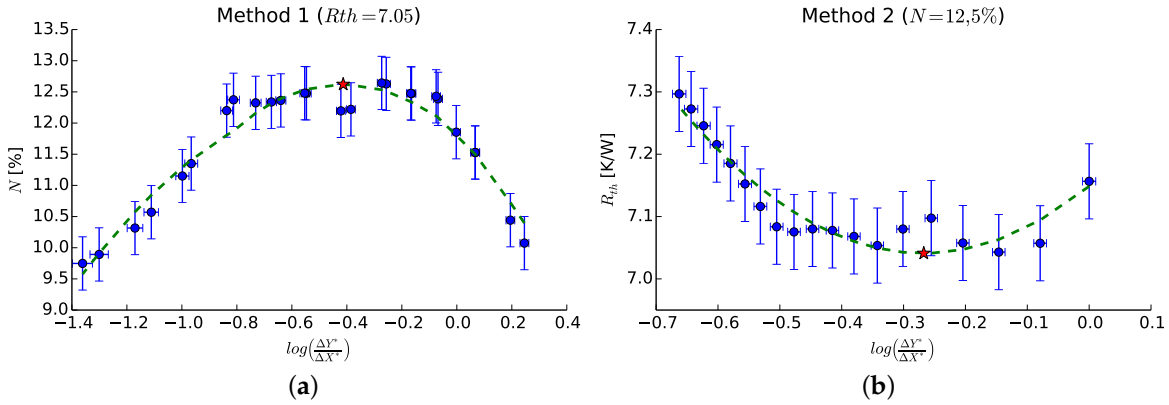

(**a**) (**b**)

Figure 7. (**a**) Heat source density along an isoline for a constant thermal resistance; and (**b**) the thermal resistance along the corresponding isoline for the density. Optima are indicated by the red stars.

The optimal thermal resistance is dependent on the desired heat source density, and is presented in Figure 8. It increases almost linearly. The changes in the slope for the optimal density—observed at a density of around 15%—are attributed to measurement artefacts, and remain within the confidence interval. The optimal line shown in Figure 8 represents the Pareto Frontier for the multi-objective problem.

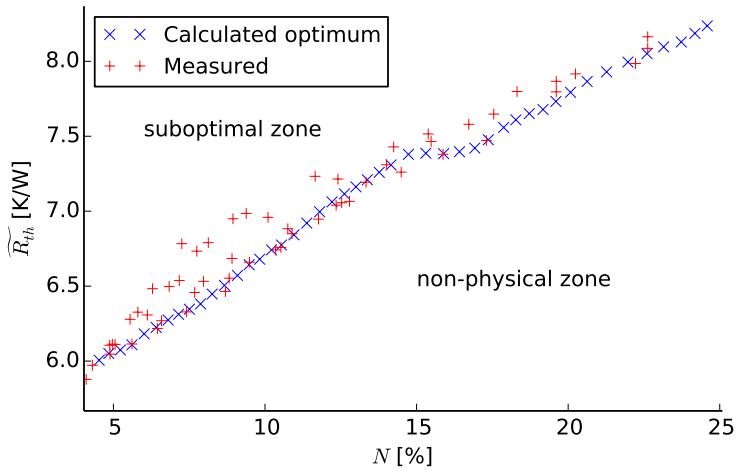

Figure 8. Measured thermal resistance and estimated thermal resistance at optimal positions.

The optimal horizontal and vertical spacing are shown in Figure 9. Both methods gave similar results, although Method 2 seems to be more robust. As expected, both the vertical and the horizontal spacings should be reduced when increasing the objective for the heat source density. The variation in the vertical direction is more than twice as fast as in the horizontal direction. It appears that the vertical spacing is converging towards 1.8 for high density. In the same way, the optimal horizontal spacing is decreasing towards zero.

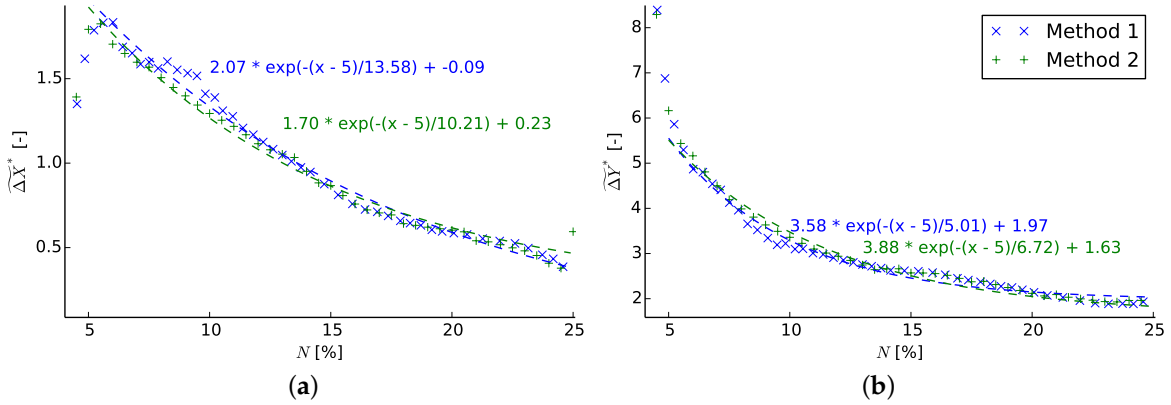

Figure 9. Optimal positions as a function of the objective heat source density. The optimal spacing is presented in the (**a**) horizontal direction and the (**b**) vertical direction.

It is observed that at low density, the optimal spacing features surprisingly diverging trends. It should be noticed that at low density, the heat sources can almost be considered as thermally independent, except for extremely low or high aspect ratios. Hence, it does not make much sense to define optima for low density, as a large range of positions are nearly optimal.

When defined as the centre-to-centre aspect ratio, the optimal ratio (see Figure 10) is almost constant and close to a mean value of 2. It increases slightly with an increasing density. In other words, the vertical spacing always needs to be larger than the horizontal spacing, due to the convective thermal coupling in the vertical direction, especially for high density.

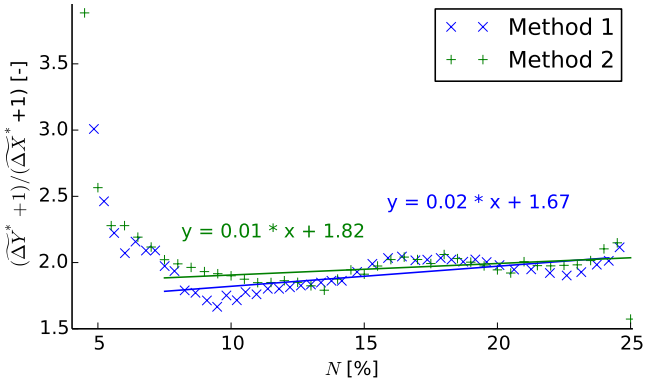

Figure 10. Optimal centre-to-centre aspect ratio as a function of the objective heat source density.

4. Discussion

Results for low and high density (i.e., below 5% and above 25%) must be approached with caution. They correspond to the corner of the plot in Figure 6, and the corresponding isolines are based on a limited number of measurement points. Adding some measurement points for high density could improve the results. The use of a Design of Experiment (DOE) method might be valuable to achieve this. However, as mentioned in Section 3.1, the thermal resistance doubled for a heat source density above 25%, compared to a single heat source case. Therefore, this range of density is probably not relevant for real cases. Likewise, low density regions correspond to a single heat source, and any optimization is meaningless.

Different shapes of heat sources could yield different results. This could be an interesting topic for further investigation. Different types of distribution could also be interesting. A staggered layout, in particular, is likely to give better results than the rectangular grid. However, the results are expected to be similar for the behaviour of the optimal configuration.

Unequally heated sources or heat sources of unequal size are other parameters which could give more degrees of freedom [20]. It is reasonable to expect different components to be mounted on the same heat sink, and therefore the case of heat sources with a different heat flux could be studied in the same manner as here.

For more advanced layouts and for non-identical heat sources, an optimization method with a model would be preferable to efficiently test a wide variety of solutions. In that case, the present results could be used for validation.

5. Conclusions

Passive cooling has been studied experimentally within the frame of an array of heat sources distributed on a regular grid. The findings for this simple and common configuration could be applied to a wide variety of thermal engineering problems. The results showed that lower density logically leads to a better cooling capacity. This obvious trend was quantified, and it appears that the thermal resistance is proportional to the square root of heat source density. This gives a simple and helpful indication for the design of compact devices with thermal constraints. It is therefore recommended that the heat sources should not cover more than 25% of the area, in order to keep the thermal resistance at a reasonably low level.

The cooling was successfully optimized by tuning the vertical and horizontal spacing. This multi-objective optimization aimed to maximize the cooling capacity (or minimize the thermal resistance), and at the same time to maximize the heat source density (i.e., minimize the construction costs, which correspond to the used area). It was also established that:

- the optimal vertical spacing varies faster than in the horizontal direction, due to convective thermal coupling;
- the vertical spacing should be approximately twice as large as the horizontal spacing;
- the optimal ratio is almost independent of the heat source density;
- for higher densities, a slight increase was noticed for the optimal ratio as a function of the objective density.

Acknowledgments: This work was supported by SweGRIDS, KIC InnoEnergy and StandUP for Energy.

Author Contributions: Antoine Baudoin has done most of the work in this study and is the main author; Antoine Baudoin and Didier Saury conceived and designed the experiment; Antoine Baudoin and Bo Zhu performed the experiments; all authors have worked on this manuscript together and all authors read and approved this manuscript.

Conflicts of Interest: The authors declare no conflict of interest.

Abbreviations

The following abbreviations and symbols are used in this manuscript:

g	Gravitational constant	m/s^2
L	Heat source width	m
H	Heat source height	m
N	Heat source density	%
U	Voltage	V
I	Current	A
R_{th}	Thermal resistance	K/W
α	Thermal diffusivity	m^2/s
β	Volumetric thermal expansion coefficient	K^{-1}
ΔX , ΔY	Horizontal and vertical spacing	m
$\Delta X^* = \Delta X/L$	Dimensionless horizontal spacing	-
$\Delta Y^* = \Delta Y/H$	Dimensionless vertical spacing	-
$\widetilde{\Delta X}^*$, $\widetilde{\Delta Y}^*$	Optimal spacing	-
ΔT	Temperature excess ($T - T_\infty$)	K
λ	Thermal conductivity	W/m.K
ν	Kinematic viscosity	m^2/s

References

1. Barstow, S. F.; Haug, O.; Krogstad, H. E. Satellite altimeter data in wave energy studies. In Proceedings of the Third International Symposium Waves, Virginia Beach, VA, USA, 3–7 November 1997.
2. Falnes, J. A review of wave-energy extraction. *Mar. Struct.* **2007**, *20*, 185–201.
3. Sjolte, J.; Tjensvoll, G.; Molinas, M. Power collection from wave energy farms. *Appl. Sci.* **2013**, *3*, 420–436.
4. Ekström, R.; Baudoin, A.; Rahm, M.; Leijon, M. Marine substation design for grid-connection of a research wave power plant on the swedish west coast. In Proceedings of the 10th European Wave and Tidal Conference (EWTEC), Aalborg, Denmark, 2–5 September 2013.
5. Müller, N.; Kouro, S.; Glaria, J.; Malinowski, M. Medium-voltage power converter interface for wave dragon wave energy conversion system. In Proceedings of the IEEE Energy Conversion Congress and Exposition, Denver, CO, USA, 15–19 September 2013.
6. Ma, K.; Liserre, M.; Blaabjerg, F.; Kerekes, T. Thermal loading and lifetime estimation for power device considering mission profiles in wind power converter. *IEEE Trans. Power Electron.* **2015**, *30*, 590–602.
7. Kovaltchouk, T.; Aubry, J.; Multon, B.; Ahmed, H.B. Influence of igbt current rating on the thermal cycling lifetime of a power electronic active rectifier in a direct wave energy converter. In Proceedings of the 2013 15th European Conference on Power Electronics and Applications (EPE), Lille, France, 2–6 September 2013.
8. Sjolte, J.; Tjensvoll, G.; Molinas, M. Reliability analysis of igbt inverter for wave energy converter with focus on thermal cycling. In Proceedings of the 2014 Ninth International Conference on Ecological Vehicles and Renewable Energies (EVER), Monte-Carlo, Monaco, 25–27 March 2014.
9. Baudoin, A.; Boström, C. Thermal modelling of a passively cooled inverter for wave power. *IET Renew. Power Gener.* **2015**, *9*, 389–395.
10. Faghri, A. Heat pipes: Review, opportunities and challenges. *Front. Heat Pipes (FHP)* **2014**, *5*, doi:10.5098/fhp.5.1.
11. Chowdhury, I.; Prasher, R.; Lofgreen, K.; Chrysler, G.; Narasimhan, S.; Mahajan, R.; Koester, D.; Alley, R.; Venkatasubramanian, R. On-chip cooling by superlattice-based thin-film thermoelectrics. *Nat. Nanotechnol.* **2009**, *4*, 235–238, .
12. Gururatana, S. Heat transfer augmentation for electronic cooling. *Am. J. Appl. Sci.* **2012**, *9*, 436.
13. Royne, A.; Dey, C.J.; Mills, D.R. Cooling of photovoltaic cells under concentrated illumination: A critical review. *Solar Energy Mater. Solar Cells* **2005**, *86*, 451–483.
14. Le Masson, S.; Nörtershäuser, D.; Mondieig, D.; Louahlia-Gualous, H. Towards passive cooling solutions for mobile access network. *Ann. Telecommun.* **2012**, *67*, 125–132.
15. Huaiyu, Y.; Koh, S.; van Zeijl, H.; Gielen, A.; Guoqi, Z. A review of passive thermal management of led module. *J. Semicond.* **2011**, *32*, 014008.
16. Baïri, A.; Zarco-Pernia, E.; De María, J.-M.G. A review on natural convection in enclosures for engineering applications. The particular case of the parallelogrammic diode cavity. *Appl. Therm. Eng.* **2014**, *63*, 304–322.
17. Heindel, T.; Ramadhyani, S.; Incropera, F. Conjugate natural convection from an array of discrete heat sources: Part 1—two-and three-dimensional model validation. *Int. J. Heat Fluid Flow* **1995**, *16*, 501–510.
18. Tou, S.; Tso, C.; Zhang, X. 3-d numerical analysis of natural convective liquid cooling of a 3×3 heater array in rectangular enclosures. *Int. J. Heat Mass Transf.* **1999**, *42*, 3231–3244.
19. Sudhakar, T.; Balaji, C.; Venkateshan, S. A heuristic approach to optimal arrangement of multiple heat sources under conjugate natural convection. *Int. J. Heat Mass Transf.* **2010**, *53*, 431–444.
20. Hotta T.K.; Venkateshan, S.P. Optimal distribution of discrete heat sources under natural convection using ann–ga based technique. *Heat Transf. Eng.* **2015**, *36*, 200–211.
21. Sudhakar, T.; Shori, A.; Balaji, C.; Venkateshan, S. Optimal heat distribution among discrete protruding heat sources in a vertical duct: A combined numerical and experimental study. *J. Heat Transf.* **2010**, *132*, 011401.
22. Habib, M.; Said, S.; Ayinde, T. Characteristics of natural convection heat transfer in an array of discrete heat sources. *Exp. Heat Transf.* **2014**, *27*, 91–111.
23. Sultan, G. Enhancing forced convection heat transfer from multiple protruding heat sources simulating electronic components in a horizontal channel by passive cooling. *Microelectron. J.* **2000**, *31*, 773–779.
24. Rajkumar, M.; Venugopal, G.; Lal, S.A. Natural convection from free standing tandem planar heat sources in a vertical channel. *Appl. Therm. Eng.* **2013**, *50*, 1386–1395.

25. Andreozzi, A.; Manca, O. Radiation effects on natural convection in a vertical channel with an auxiliary plate. *Int. J. Therm. Sci.* **2015**, *97*, 41–55.
26. Hajmohammadi, M.; Nourazar, S.; Campo, A.; Poozesh, S. Optimal discrete distribution of heat flux elements for in-tube laminar forced convection. *Int. J. Heat Fluid Flow* **2013**, *40*, 89–96.
27. Öztop, H.F.; Estellé, P.; Yan, W.-M.; Al-Salem, K.; Orfi, J.; Mahian, O. A brief review of natural convection in enclosures under localized heating with and without nanofluids. *Int. Commun. Heat Mass Transf.* **2015**, *60*, 37–44.
28. Narasimham, G. Natural convection from discrete heat sources in enclosures: An overview. *Vivechan Int. J. Res.* **2010**, *1*, 63–78.
29. Da Silva, A.; Lorente, S.; Bejan, A. Optimal distribution of discrete heat sources on a wall with natural convection. *Int. J. Heat Mass Transf.* **2004**, *47*, 203–214.

© 2016 by the authors; licensee MDPI, Basel, Switzerland. This article is an open access article distributed under the terms and conditions of the Creative Commons Attribution (CC-BY) license (http://creativecommons.org/licenses/by/4.0/).